Insight into the Underlying Synergy between Exo–Lytic Cellulases

Zhiyou Zong
Nankai University
Qiyu Li
Nankai University
Zhangyong Hong
Nankai University
Wensheng Cai (wscai@nankai.edu.cn)
Nankai University
Xueguang Shao
Nankai University

Research Article

Keywords: Cellulases, Lignocellulose, Synergy, Enzyme–enzyme interactions

Posted Date: March 16th, 2021

DOI: https://doi.org/10.21203/rs.3.rs-298025/v1

Abstract

Lignocellulosic biomass can be converted into biofuels and biochemicals, through a synergetic degradation by cellulases. The underlying cooperative mechanism is of paramount importance for the development of efficient enzyme cocktails. The synergy between exo–lytic cellulases, however, still remains poorly understood. In the present contribution, we decipher the synergism by investigation of the enzyme–enzyme interactions (EEIs) between two exo–lytic cellulases––*Talaromyces emersonii* Cel7A (*Te*Cel7A) and *Trichoderma reesei* Cel6A (*Tr*Cel6A), and between *Te*Cel7A and other main components in the cocktails, and propose a novel synergistic way. The enzymes are found to be apt to bind around the eight substrate–enclosing loops (SELs) of *Te*Cel7A, of which the *Tr*Cel6A possesses the strongest binding energy with *Te*Cel7A. The combination between *Te*Cel7A and *Tr*Cel6A is further investigated experimentally by Microscale Thermophoresis, confirming the existence of their interactions. Due to the EEIs, the flexibility of the SELs, which mediate dissociation of *Te*Cel7A from cellulose, is increased. We further found that the improved flexibility of loop B3 is pivotal to accelerate dethreading process, helping improving enzymatic hydrolytic efficiency. In view of our theoretical and experimental results here and previous experimental phenomena, the carbohydrate binding modules of the exo–lytic enzymes, which enable them to absorb on the same plane of the substrate, are conjectured to enhance the degree of the EEIs. This work brings to light an underlying synergy between exo–lytic cellulases, and is conducive to a systematic understanding of the synergetic actions in cellulase cocktails.

Introduction

Lignocellulosic biomass can be converted into many value–added products, providing prominent economic and environmental benefits [1–3]. Enzymatic hydrolysis has emerged as one of the most significant technologies for the conversion of the biomass into glucose [4]. To complete hydrolysis of the complex natural substrate, a variety of enzymes with different specificities, such as endo–beta–1,4–glucanases (EGs, EC 3.2.1.4), cellobiohydrolases (CBHs, EC 3.2.1.91) and beta–glucosidases (BGs, EC 3.2.1.21), acting in synergy, are required. How to degrade efficiently the biomass by cellulase cocktails was, therefore, investigated widely to design optimal enzymatic combinations and ratios [5–7].

Cellulose, the most important component of lignocellulose can be degraded gradually into glucose by three steps, i.e., (i) EGs cleave randomly β–1,4 linkages of the cellulosic chains, producing reducing or non–reducing ends, (ii) CBHs assault the cellulose chain from these ends, yielding cellobioses, and (iii) BGs eventually convert cellobiose to glucoses [8–12]. Furthermore, EG can remove amorphous–unordered substrate areas, hence helping cellobiohydrolase I (CBHI or Cel7A) interact well with cellulosic substrate [13–15]. In the work of Ng et al., BG was found to alleviate the inhibition of cellobiose on CBHI [16]. This sort of synergism, resulting from the positive effect of EG or BG on the degradation of cellulose by CBHI was widely recognized [17].

According to the study of Trudeau et al., substantial cooperation between exo–lytic enzymes, i.e., CBHI and cellobiohydrolase II (CBHII or Cel6A) also exists [14], whereas the mechanism is poorly understood

[18–21]. The rate of glycoside hydrolase family 7 (GH7) CBHI leaving cellulose after catalysis, namely dissociation rate is known to be the rate–limiting step when employed alone [22–29]. The high flexibility of the substrate–enclosing loops (SELs, Fig. 1) has been proved to accelerate enzymatic dissociation, improving the yield of cellobiose [30, 31]. Furthermore, it has been reported that the activity of cellulase can be increased or decreased by the structural changes due to the association with other proteins or ligands [32–34]. It is, therefore, reasonable to believe that the cooperation between the two exo–lytic cellulases may arise from the influence of CBHII on the flexibility of SELs in CBHI by enzyme–enzyme interactions (EEIs).

GH7 CBHIs are one of the most abundant enzymes in native fungal secretions [35, 36]. The structure and function of these enzymes, especially *Trichoderma reesei* (*T. reesei*) CBHI and *Talaromyces emersonii* CBHI (*Te*Cel7A) have been deciphered clearly by crystallography and molecular dynamics (MD) simulations [37–40], making them excellent model systems. In the present work, the relevant molecular–level synergetic mechanism of exo–lytic cellulases– *Te*Cel7A and *T. reesei* CBHII (*Tr*Cel6A) was deciphered using docking, MD simulations and Microscale Thermophoresis (MST) experiment. In brief, this work provides useful insight into the synergetic actions between cellulases.

Results And Discussion

Enzyme–Enzyme Docking and Interactional Energy

HADDOCK [41] was employed to investigate the EEIs of *Te*Cel7A with *Tr*Cel6A, EG, BG and *Te*Cel7A itself, respectively. Table 1 shows the docking results for these assemblies, wherein *Te*Cel7A–EG processes the best Z–score. Binding affinity (ΔG) and the dissociation constant (K_d) were then measured by PRODIGY [42]. *Te*Cel7A– *Tr*Cel6A features the strongest affinity of − 17.2 kcal/mol. These results suggest that the two enzymes can interact powerfully, mainly owing to their flexible SELs (see Fig. 1). However, *Te*Cel7A is not apt to bind with itself in view of the lowest HADDOCK score, Z–Score and binding affinity of *Te*Cel7A– *Te*Cel7A assembly, compared with the other enzyme–enzyme complexes.

Table 1
Results of HADDOCK for assemblies of *Te*Cel7A with *Tr*Cel6A, EG, BG and *Te*Cel7A itself.

	***Te*Cel7A– *Tr*Cel6A**	***Te*Cel7A–EG**	***Te*Cel7A–BG**	***Te*Cel7A– *Te*Cel7A**
HADDOCK score	−57.3 ± 11.5	−92.9 ± 3.8	−59.3 ± 7.8	−40.7 ± 3.9
Z–Score	−2.1	−2.7	−1.9	−0.8
ΔG (kacl/mol)	−17.2	−12.7	−15.3	−10.5

On the basis of protein–protein docking, multi–microsecond MD simulations were then employed to decipher their underlying mechanism in detail. The four initial structures of *Te*Cel7A, *Tr*Cel6A, EG, BG and the four protein-protein complexes of *Te*Cel7A– *Tr*Cel6A, *Te*Cel7A–EG, *Te*Cel7A–BG and *Te*Cel7A– *Te*Cel7A were sufficiently relaxed in an explicit water environment and each followed by a 500 ns MD

simulation, except for *Te*Cel7A– *Tr*Cel6A, which followed by 1.5 μs. The evolution of the center-of-mass (COM) distance between the two proteins in each complex structure (Fig. S1) suggests that the well-equilibrated states have been reached. As reported in Table 2, the binding free energies calculated by the MM-PBSA method indicate that the two exo–lytic cellulases possess the strongest binding free energy among the four enzyme-enzyme assemblies. In view of results of docking and MD simulations, we therefore suggest that *Tr*Cel6A is the most promising one to influence the hydrolytic function of *Te*Cel7A.

Table 2
Binding free energies[a] for enzyme–enzyme complexes.

System	ΔG	ΔE_{MM}[b]	ΔG_{PB}	ΔG_{SA}
*Te*Cel7A-*Tr*Cel6A	-23.4	-1232.2	-3207.8	-2.1
*Te*Cel7A-EG	-7.8	-519.6	-996.1	-48.4
*Te*Cel7A-BG	-16.2	-158.0	-3076.4	-14.8
*Te*Cel7A-*Te*Cel7A	-14.6	-284.1	-2562.7	-69.1

[a] All quantities are in kcal mol^{-1}. [b] ΔE_{MM} energy includes the intermolecular noncovalent interactions and the change of the conformational energies.

Binding Modes and Interaction Interface of Te**Cel7A–**Tr**Cel6A**

As depicted in Fig. 2a, the optimal docking pose for *Te*Cel7A– *Tr*Cel6A indicates that the two exo–lytic cellulases bind with each other with their SELs. Furthermore, the other enzymes were found to combine to the region around SELs of *Te*Cel7A as well (Fig. S2). Eight hydrophobic residues in *Te*Cel7A (Ala375, Ala376, Met378, Leu379, Ala389, Ile396, Ala397 and Val407) were found to locate at the interactional interfaces of the complexes (Fig. 2b). It is well known that the unproductive adsorption caused by the binding of hydrophobic sites between cellulases and lignin is one of the main limiting factors in the enzymatic hydrolysis [23, 43]. EEIs can properly prevent cellulases from the adsorption of lignin residues, thereby contributing to increasing the efficiency of enzymatic hydrolysis.

Influence of Tr**Cel6A on Flexibility and Catalytic Region of** Te**Cel7A**

As depicted in Fig. 3a, the interactional interface of *Te*Cel7A– *Tr*Cel6A is changed after 1.5 μs MD simulation, like that of other enzyme-enzyme complexes (Fig. S3). The phenomena indicate that this nonspecific association between enzymes cannot always sustain. Since the enzymes should work on their exclusive substrates by traditional synergetic forms, we, therefore, suggest that the separation of the enzyme-enzyme complexes after EEIs is beneficial to hydrolysis cycle. Figure 3b shows the root mean square fluctuation (RMSF) values of the residues in *Te*Cel7A with and without combining *Tr*Cel6A. It is apparent that flexibility of the loops A1, B1, B2 and B3 is improved significantly by EEIs. In the enzymatic hydrolysis, improved flexibility of the SELs will accelerate dissociation – the rate–limiting step of GH7 CBHI degrading cellulose alone, increasing the yield of cellobiose.

It is acknowledged that the initial binding of *Te*Cel7A to cellulose is certainly influenced by the opening of SELs [44, 45]. As shown in Fig. 4a, the cross–sectional area (CSA) formed by the center of mass (COM) distances of loops B2, B3 and A3 were measured. Figure 4b indicates that the CSA of *Te*Cel7A is expanded notably by association with *Tr*Cel6A. Before the degradation of lignocellulose by *Te*Cel7A, the EEIs between the two exo–lytic cellulases in hydrolytic system will help the initial association of *Te*Cel7A with cellulose. Andersen et al. have reported that the highest synergy was observed at the beginning of hydrolysis [46], consistent with our theoretical analysis.

Dethreading Process

Vermaas et al. have reported that dethreading is the predominant mechanism for dissociation of GH7 CBHI from cellulose [30]. We, therefore, speculate that highly extent of synergy between the two exo–lytic cellulases occurs in dethreading process − the longest time-consuming action of GH7 CBHI degrading cellulose. As shown in Fig. 5a, loops A1, B1 and B2 absorb on the surface of cellulose before dissociation. The notably improved flexibility of these three loops after EEIs (see Fig. 3b) can enhance motility of CBHI, helping the enzyme leave the surface of substrate. The results of Vermaas et al. further indicate that − 1 to − 3 transition is the rate–limiting step for dethreading, especially − 1 to − 2 [30]. As illustrated in Fig. 5b, many hydrogen bonds are formed between − 1 glucosyl ring and the enzyme, influencing the rate of dethreading significantly. Acceleration of dethreading was deemed to depend on modulating interactions around the − 1 state [30]. Loop B3, closest to the − 1 site is, therefore, the most promising SEL to influence dethreading. In view of the improved flexibility of loop B3 (see Fig. 3b) after EEIs, it will interact with − 1 glucosyl ring frequently, facilitating motion of the substrate. We, therefore, suggest that the key to the synergy of exo–lytic cellulases is to improve the flexibility of loop B3, thus accelerating dethreading.

Existence of EEIs and the Role of Carbohydrate Binding Module (CBM)

To verify the existence of combination between exo–lytic cellulases experimentally, MST experiment were performed, characterizing the binding of *Te*Cel7A to *Tr*Cel6A. The relevant result indicates that the interactions of *Te*Cel7A with *Tr*Cel6A exist, but weak (Kd = 140 ± 60 μM, see Fig. 6). In view of the result of Fig. 3a and the corresponding theoretical analysis, the weak combination between exo–lytic cellulases is conjectured to be reasonable. The degree of cooperation between them is, therefore, suggested to depend on the frequency of EEIs. In the study of Badino et al., the synergetic extent of the two exo–lytic cellulases achieved the highest level when both the two enzymes possess CBMs [21]. In addition, their synergy was decreased step by step if one or both of them do not have CBMs [21]. We conjecture that CBMs can enable the two exo–lytic cellulases to locate at the surface of cellulose to interact adequately, enhancing the degree of EEIs. Overall, the synergy between the exo–lytic cellulases can arise from increased flexibility of the key loops in *Te*Cel7A by EEIs, degree of which is improved by their CBMs.

Conclusions

In the present work, we deciphered the molecular–level mechanism of synergy between exo–lytic cellulases by docking, microsecond–time scale MD simulations and MST experiment. Flexibility of SELs in CBHI mediates its dissociation from cellulose, and highly flexible SELs, especially loop B3, induced by EEIs is the crucial cause for the synergy between exo–lytic cellulases. Furthermore, EEIs can also decrease unproductive adsorption and open catalytic domain, help improve the efficiency of CBHI. CBMs which enable the exo–lytic cellulases to interact frequently, enhance the degree of their synergy. Put together, this work represents a step forward in the understanding of the synergistic actions in enzymatic hydrolysis, and is expected to contribute to the more efficient degradation of lignocellulose by cellulase cocktails.

Experimental

Docking and Simulation Details

The crystal structures of EG (PDB code 1KS5), *Te*Cel7A (PDB code 3PFX) and *Tr*Cel6A (PDB code 1HGW, in which A175 was mutated back to Asp) were obtained from protein data bank (PDB). BG, secreted by *Penicillium piceum*, was homologically modeled by SWISS-MODEL (swissmodel.expasy.org) [47–51]. The templates, PDB codes 3ZYZ and 4IIB, have the highest homology with the target BG. The protein–protein dockings of *Te*Cel7A– *Tr*Cel6A, *Te*Cel7A–EG, *Te*Cel7A–BG and *Te*Cel7A– *Te*Cel7A were carried out by HADDOCK to obtain the optimal binding poses.

MD simulations were then carried out for the four individual enzymes and the four protein–protein complexes. All the assemblies were solvated in an equilibrated box of water separately. The overall charge neutrality was achieved by adding Na^+ ions to the solution. Each molecular system before production simulations underwent i) 5000 steps minimization and 100 ps MD simulation with protein restrained, and ii) 5 ns of water equilibration without restrained. The interactions of the four assemblies were investigated by performing a total of 6 μs MD simulations. The details of the molecular assemblies are provided in Table S1. The scalable program NAMD 2.13 [52] with the CHARMM36 force field [53–55], and the TIP3P water model [56] were used to perform the MD simulations. Visualization and analysis of all the MD trajectories were carried out with the VMD program [57]. Binding free energies of these complexes using MM-PBSA method were calculated as described in our previous work [33].

MST Experiment

*Te*Cel7A and *Tr*Cel6A were expressed and purified as described in our previous work [40]. *Tr*Cel6A was labeled with NT-647-NHS (NanoTemper Technologies GmbH, Munich, Germany) at a dye-to-protein ratio of 3:1 and purified with a 1 mL Pierce® Desalting Column (Thermo Scientific) using citrate buffer (10 mM Sodium Citrate, 100 nM NaCl, 0.05% Tween 20, pH 5.0) as the buffer. Capillaries were loaded with 20 nM NT-647-NHS labeled *Tr*Cel6A and 16 concentrations of *Te*Cel7A from 12.4 nM to 407 μM in citrate buffer (10 mM Sodium Citrate, 100 nM NaCl, 0.05% Tween 20, pH 5.0). MST measurements were taken using

Monolith NT.115(NanoTemper Technologies GmbH, Munich, Germany) at room temperature. The data was handled using Software Manual MO. Affinity Analysis and MO. Control.

Declarations

Acknowledgements

This study was supported by the National Natural Science Foundation of China (21773125 and 21775076, 22005157), and the Fundamental Research Funds for the Central Universities, Nankai University (63201043). Z. Z. gratefully acknowledges the financial support from China Scholarship Council (201706205014). The FP7 WeNMR (261572), H2020 West–Life (675858) and the EOSC–hub (777536) European e–Infrastructure projects are acknowledged for the use of their web portals, which make use of the EGI infrastructure with the dedicated support of CESNET–MetaCloud, INFN–PADOVA, NCG–INGRID–PT, TW–NCHC, SURFsara and NIKHEF, and the additional support of the national GRID Initiatives of Belgium, France, Italy, Germany, the Netherlands, Poland, Portugal, Spain, UK, Taiwan and the US Open Science Grid.

Funding

This study was funded by National Natural Science Foundation of China 21773125 to WSC, 21775076 to XGS and 22005157 to ZYZ, and funded by the Fundamental Research Funds for the Central Universities, Nankai University 63201043 to ZYZ.

Conflict of Interest

The authors declare that they have no conflict of interest.

Availability of data and materials

Simulation details, center-of-mass distance of two proteins in each complex, optimal docking poses and final states after MD simulations of *Te*Cel7A–EG, *Te*Cel7A–BG and *Te*Cel7A– *Te*Cel7A are available in Supplementary Information.

Code availability

Not applicable.

Author's Contributions

WSC, XGS ZYH and ZYZ designed the research. ZYZ and QYL did the simulations and experiment, respectively. WSC and ZYZ wrote the manuscript and analyzed the data.

Ethical Approval

Not applicable.

Consent to participate

The manuscript has not been published previously by any of the authors and is not under consideration for publication in another journal at the time of submission.

Consent for publication

All authors have read the manuscript and approved to submit to this journal.

References

1. Zhu Y, Li Z, Chen J (2019) Applications of lignin-derived catalysts for green synthesis. Green Energy Environ. 4:210–244. DOI: 1016/j.gee.2019.01.003
2. Himmel ME, Ding SY, Johnson DK, Adney WS, Nimlos MR, Brady JW, Foust TD (2007) Biomass recalcitrance: engineering plants and enzymes for biofuels production. Science 315: 804–807. DOI:1126/science.1137016
3. Chundawat SP, Beckham GT, Himmel ME, Dale BE (2011) Deconstruction of Lignocellulosic Biomass to Fuels and Chemicals. Annu Rev Chem Biomol Eng 2:121–145. DOI:1146/annurev-chembioeng-061010-114205
4. Van Dyk JS, Pletschke BI (2012) A review of lignocellulose bioconversion using enzymatic hydrolysis and synergistic cooperation between enzymes—Factors affecting enzymes, conversion and synergy. Biotechnol Adv 30:1458– DOI: 10.1016/j.biotechadv.2012.03.002
5. Olsen JP, Borch K, Westh P (2017) Endo/exo-synergism of cellulases increases with substrate conversion. Biotechnol Bioeng 114:696–700. DOI: 10.1002/bit.26179
6. Li J, Zhou P, Liu H, Xiong C, Lin J, Xiao W, Gong Y, Liu Z (2014) Synergism of cellulase, xylanase, and pectinase on hydrolyzing sugarcane bagasse resulting from different pretreatment technologies. Bioresource Technol 155:258–265. DOI: 10.1016/j.biortech.2013.12.113
7. Hu J, Gourlay K, Arantes V, Van Dyk JS, Pribowo A, Saddler JN (2015) The accessible cellulose surface influences cellulase synergism during the hydrolysis of lignocellulosic substrates. ChemSusChem 8:901–907. DOI: 10.1002/cssc.201403335
8. Bansal P, Hall M, Realff MJ, Lee JH, Bommarius AS (2009) Modeling cellulase kinetics on lignocellulosic substrate Biotechnol Adv 27:833–848. DOI: 10.1016/j.biotechadv.2009.06.005
9. Henrissat B (1994) Cellulases and their interaction with cellulose. Cellulose 1:169–196. https://doi.org/10.1007/BF00813506
10. Lynd LR, Weimer PJ, van Zyl WH, Pretorius IS (2002) Microbial Cellulose Utilization: Fundamentals and Biotechnology. Microbiol Mol Biol R 66:506–5 DOI: 10.1128/mmbr.66.3.506-577.2002
11. Teeri TT (1997) Crystalline cellulose degradation: new insight into the function of cellobiohydrolas Trends Biotechnol 15:160–167. https://doi.org/10.1016/S0167-7799(97)01032-9

12. Zhang YHP, Lynd LR (2004) Toward an aggregated understanding of enzymatic hydrolysis of cellulose: noncomplexed cellulase syste Biotechnol Bioeng 88:797–824. https://doi.org/10.1002/bit.20282
13. Jalak J, Kurašin M, Teugjas H, Väljamäe P (2012) Endo-exo Synergism in Cellulose Hydrolysis Revisited. J Biol Chem 287:28802–28815. DOI: 10.1074/jbc.m112.381624
14. Trudeau DL, Lee TM, Arnold FH (2015) Engineered thermostable fungal cellulases exhibit efficient synergistic cellulose hydrolysis at elevated temperatures. Biotechnol Bioeng 111:2390–2397. DOI: 10.1002/bit.25308
15. Ganner T, Bubner P, Eibinger M, Mayrhofer C, Plank H, Nidetzky B (2012) Dissecting and reconstructing synergism: in situ visualization of cooperativity among cellu J Biol Chem 287: 43215–43222. DOI: 10.1074/jbc.M112.419952
16. Ng IS, Tsai SW, Ju YM, Yu SM, Ho TH (2011) Dynamic synergistic effect on *Trichoderma reesei* cellulases by novel b-glucosidases from *Taiwanese fungi*. Bioresource Technol 102:6073–6081. DOI: 10.1016/j.biortech.2010.12.110
17. Wood TM, McCrae SI (1978) The cellulase of Trichoderma koningii. Purification and properties of endoglucanase components with special reference to their action on cellulase when acting alone or in synergism with the cellobiohydrolase. Biochem J 171:61–72. DOI: 10.1042/bj1710061
18. Henrissat B, Teeri TT, Warren RA (1998) A scheme for designating enzymes that hydrolyse the polysaccharides in the cell walls of plants. FEBS Lett 425:352–354. DOI: 10.1016/S0014-5793(98)00265-8
19. Koivula A, Ruohonen L, Wohlfahrt G et al (2002) The active site of cellobiohydrolase Cel6A from Trichoderma reesei: The roles of aspartic acids D221 and D175. J Am Chem Soc 124:10015–10024. DOI: 10.1021/ja012659q
20. Igarashi K, Uchihashi T, Koivula A, Wada M, Kimura S, Okamoto T, Penttilä M, Ando T, Samejima M (2011) Traffic jams reduce hydrolytic efficiency of cellulase on cellulose surfac Science 333:1279–1282. DOI: 10.1126/science.1208386
21. Badino SF, Christensen SJ, Kari J, Windahl MS, Hvidt S, Borch K, Westh P (2017) Exo-exo synergy between Cel6A and Cel7A from Hypocrea jecorina: Role of carbohydrate binding module and the endo-lytic character of the enzymes. Biotechnol Bioeng 114:1639–1647. DOI: 10.1002/bit.26276
22. Payne CM, Knott BC, Mayes HB, Hansson H, Himmel ME, Sandgren M, Ståhlberg J, Beckham GT (2015) Fungal Cellulases. Chem Rev 115:1308–1448. DOI: 10.1021/cr500351c
23. Kurasin M, Valjamae P (2011) Processivity of cellobiohydrolases is limited by the substrate. J Biol Chem 286:169–177. DOI: 10.1074/jbc.M110.161059
24. Cruys–Bagger N, Alasepp K, Andersen M, Ottesen J, Borch K, Westh P (2016) Rate of Threading a Cellulose Chain into the Binding Tunnel of a Cellulase. J Phys Chem B 120:5591–5600. DOI: 10.1021/acs.jpcb.6b01877
25. Kari J, Olsen J, Borch K, Cruys–Bagger N, Jensen K, Westh P (2014) Kinetics of cellobiohydrolase (Cel7A) variants with lowered substrate affinit J Biol Chem 289:32459–32468. DOI:

10.1074/jbc.M114.604264

26. Cruys–Bagger N, Elmerdahl J, Praestgaard E, Tatsumi H, Spodsberg N, Borch K, Westh P (2012) Pre-steady state kinetics for the hydrolysis of insoluble cellulose by cellobiohydrolase Cel7A. J Biol Chem 287:18451–18458. DOI: 10.1074/jbc.M111.334946
27. Cruys–Bagger N, Tatsumi H, Ren GR, Borch K, Westh P (2013) Transient kinetics and rate-limiting steps for the processive cellobiohydrolase Cel7A: Effects of substrate structure and carbohydrate binding domain. Biochemistry 52:8938–8948. DOI: 10.1021/bi401210n
28. Levine SE, Fox JM, Blanch HW, Clark DS (2010) A mechanistic model of the enzymatic hydrolysis of cellulos Biotechnol Bioeng 107:37–51. DOI: 10.1002/bit.22789
29. Vermaas JV, Kont R, Beckham GT, Crowley MF, Gudmundsson M, Sandgren M, Ståhlberg J, Väljamäe P, Knott BC (2019) The dissociation mechanism of processive cellulas P Natl Acad Sci USA 116:23061–23067. DOI: 10.1073/pnas.1913398116
30. Taylor II LE, Knott BC, Baker JO, Alahuhta PM, Hobdey SE, Linger JG, Lunin VV, Amore A, Subramanian V, Podkaminer K et al (2018) Engineering enhanced cellobiohydrolase acti Nat Commun 9:1186. DOI: 10.1038/s41467-018-03501-8
31. Sørensen TH, Windahl MS, McBrayer B, Kari J, Olsen JP, Borch K, Westh P (2017) Loop variants of the thermophile Rasamsonia emersonii Cel7A with improved activity against cellulose. Biotechnol Bioeng 114:53–62. DOI: 10.1002/bit.26050
32. Han Y, Chen H (2007) Synergism between corn stover protein and cellulase. Enzyme Microb Technol 41:638–645. DOI: 10.1016/j.enzmictec.2007.05.012
33. Zong Z, He R, Fu H, Zhao T, Chen S, Shao X, Zhang D, Cai W (2016) Pretreating cellulases with hydrophobins for improving bioconversion of cellulose: an experimental and computational study. Green Chem 18:6666–6674. DOI: 10.1039/C6GC02694J
34. Talukder MMR, Hai YG, Puah SM (2017) Interaction of silica with cellulase and minimization of its inhibitory effect on cellulose hydrolys Biochem Eng J 118:91–96. DOI: 10.1016/j.bej.2016.11.016
35. Herpoël–Gimbert I, Margeot A, Dolla A, Jan G, MolléD, Lignon S, Mathis H, Sigoillot JC, Monot F, Asther M (2008) Comparative secretome analyses of two Trichoderma reesei RUT-C30 and CL847 hypersecretory strains. Biotechnol Biofuels 1:18–28. DOI: 10.1186/1754-6834-1-18
36. Rosgaard L, Pedersen S, Langston J, Akerhielm D, Cherry JR, Meyer AS (2007) Evaluation of minimal Trichoderma reesei cellulase mixtures on differently pretreated barley straw substr Biotechnol Progr 23:1270–1276. DOI: 10.1021/bp070329p
37. Divne C, Ståhlberg J, Reinikainen T, Ruohonen L, Pettersson G, Knowles JKC, Teeri TT, Jones TA (1994) The three-dimensional structure of the catalytic core of cellobiohydrolase I from *Trichoderma reesei*. Science 265:524. DOI: 10.1126/science.8036495
38. Knott BC, Crowley MF, Himmel ME, Ståhlberg J, Beckham GT (2014) Carbohydrateprotein interactions that drive processive polysaccharide translocation in enzymes revealed from a computational study of cellobiohydrolase processivity. J Am Chem Soc 136:8810–8819. DOI: 10.1021/ja504074g

39. Knott BC, Haddad MM, Crowley MF, Mackenzie LF, Götz AW, Sandgren M, Withers SG, Ståhlberg J, Beckham GT (2014) The mechanism of cellulose hydrolysis by a two-Step, retaining cellobiohydrolase elucidated by structural and transition path sampling stu J Am Chem Soc 136:321–329. DOI: 10.1021/ja410291u
40. Zong Z, Li Q, Hong Z, Fu H, Cai W, Chipot C, Jiang H, Zhang D, Chen S, Shao X (2019) Lysine mutation of the claw-arm-like loop accelerates catalysis by cellobiohydrolases. J Am Chem Soc 141:14451–14459. DOI: 10.1021/jacs.9b08477
41. van Zundert GCP, Rodrigues JPGLM, Trellet M, Schmitz C, Kastritis PL, Karaca E, Melquiond ASJ, van Dijk M, de Vries SJ, Bonvin AMJJ (2015) The HADDOCK2.2 web server: user-friendly integrative modeling of biomolecular complexe J Mol Biol 428:720–725. DOI: 10.1016/j.jmb.2015.09.014
42. Xue L, Rodrigues J, Kastritis P, Bonvin AMJJ, Vangone A (2016) CRISPR-ERA: a comprehensive design tool for CRISPR-mediated gene editing, repression and activation. Bioinformatics 32:3676–3678. DOI: 10.1093/bioinformatics/btv423
43. Alkasrawi M, Eriksson TJ, Wingren A, Galbe M, Tjerneld F (2003) The effect of Tween-20 on simultaneous saccharification and fermentation of softwood to eth Enzyme Microb Tech 33:71–78. DOI: 10.1016/S0141-0229(03)00087-5
44. Eriksson T, Börjesson J, Tjerneld F (2002) Mechanism of surfactant effect in enzymatic hydrolysis of lignocellulose. Enzyme Microb Tech 31:353–364. DOI: 10.1016/S0141-0229(02)00134-5
45. Bu L, Crowley MF, Himmel ME, Beckham GT (2013) Computational investigation of the pH dependence of loop flexibility and catalytic function in glycoside hydrolases. J Biol Chem 288:12175–12186. DOI: 10.1074/jbc.M113.462465
46. Andersen N, Johansen KS, Michelsen M, Stenby EH, Krogh KB, Olsson L (2008)Hydrolysis of cellulose using mono-component enzymes shows synergy during hydrolysis of phosphoric acid swollen cellulose (PASC), but competition on Avicel. Enzyme Microb Technol 42:362–370. DOI: 10.1016/j.enzmictec.2007.11.018
47. Waterhouse A, Bertoni M, Bienert S, Studer G, Tauriello G, Gumienny R, Heer FT, de Beer TAP, Rempfer C, Bordoli L, Lepore R, Schwede T (2018) SWISS-MODEL: homology modelling of protein structures and complexes. Nucleic Acids Res 46:296–303. DOI: 10.1093/nar/gky427
48. Bienert S, Waterhouse A, de Beer TAP, Tauriello G, Studer G, Bordoli L, Schwede T (2017) The SWISS-MODEL Repository—new features and functionality. Nucleic Acids Res 45:313–319. DOI: 10.1093/nar/gkw1132
49. Guex N, Peitsch MC, Schwede T (2009) Automated comparative protein structure modeling with SWISS-MODEL and Swiss-PdbViewer: A historical perspective. Electrophoresis 30:162–173. DOI: 10.1002/elps.200900140
50. Studer G, Rempfer C, Waterhouse AM, Gumienny G, Haas J, Schwede T (2020) QMEANDisCo-distance constraints applied on model quality estimation. Bioinformatics 36:1765– DOI: 10.1093/bioinformatics/btz828

51. Bertoni M, Kiefer F, Biasini M, Bordoli L, Schwede T (2017) Modeling protein quaternary structure of homo-and heterooligomers beyond binary interactions by homology. Sci Rep 7:10480. DOI: 10.1038/s41598-017-09654-8
52. Hatcher E, Guvench O, MacKerell A Jr (2009) CHARMM additive all-atom force field for acyclic polyalcohols, acyclic carbohydrates, and inositol. J Chem Theory Comput 5:1315–1329. DOI: 10.1021/ct9000608
53. Vanommeslaeghe K, Hatcher E, Acharya C, Kundu S, Zhong S, Shim J, Darian E, Guvench O, Lopes P, Vorobyov I, Mackerell JAD (2010) CHARMM general force field: a force field for drug-like molecules compatible with the CHARMM all-atom additive biological force fields. J Comput Chem 31:671–690. DOI: 10.1002/jcc.21367
54. Guvench O, Greene SN, Kamath G, Brady JW, Venable RM, Pastor RW, MacKerell AD Jr (2008) Additive empirical force field for hexopyranose monosaccharid J Comput Chem 29:2543–2564. DOI: 10.1002/jcc.21004
55. Guvench O, Hatcher E, Venable RM, Pastor RW, MacKerell AD (2009) CHARMM Additive all-atom force field for glycosidic linkages between hexopyranoses. J Chem Theory Comput 5:2353–2370. DOI: 10.1021/ct900242e
56. Jorgensen WL, Chandrasekhar J, Madura JD, Impey RW, Klein ML (1983) Comparison of simple potential functions for simulating liquid water. J Comput Phys 79:926–935. DOI: 10.1063/1.445869
57. Humphrey W, Dalke A, Schulten K (1996) VMD: visual molecular dynamics. J Mol Graph Model 14:33–38. DOI: 10.1016/0263-7855(96)00018-5

Figures

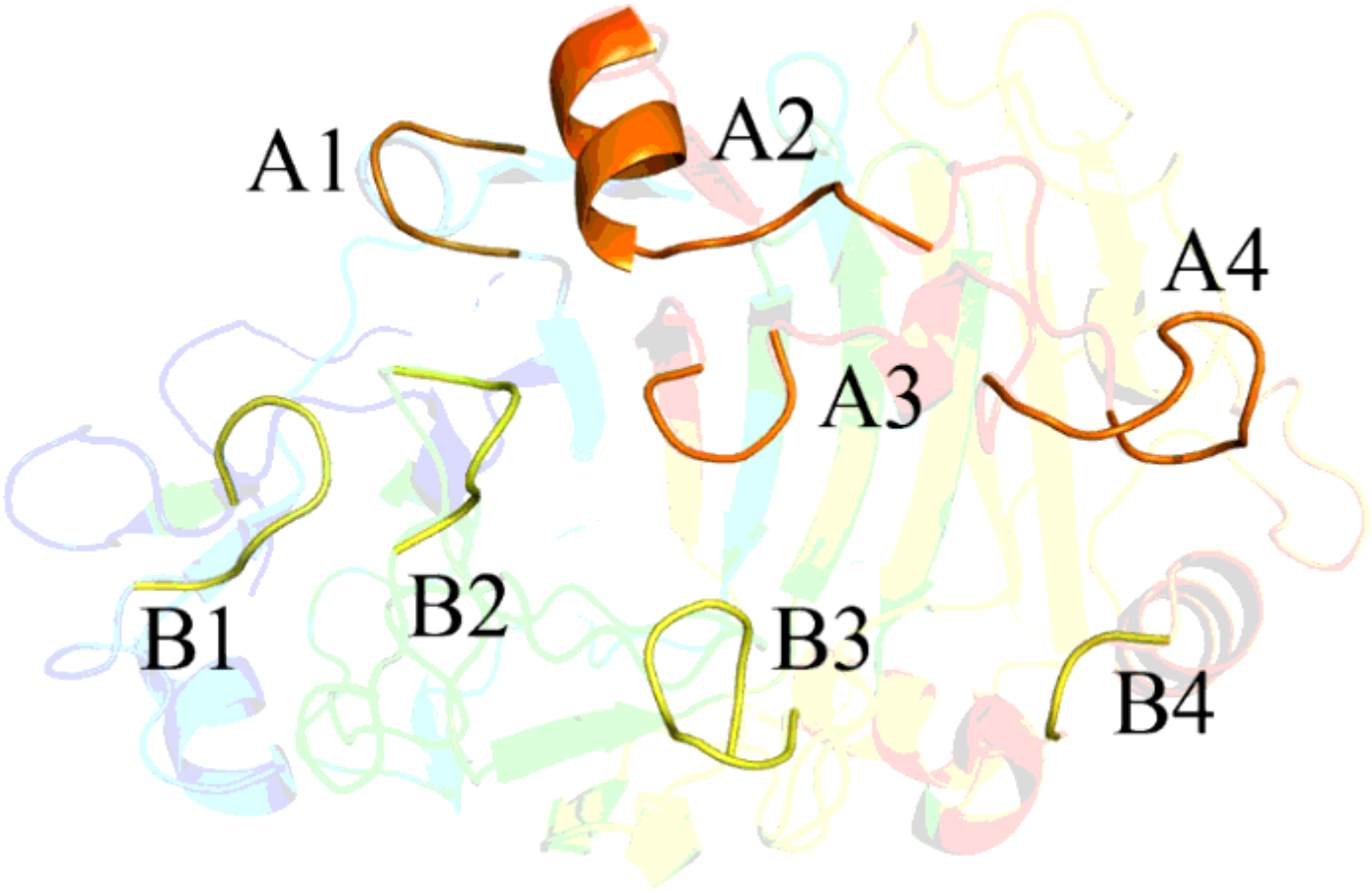

Figure 1

Structure of GH7 CBHI (PDB code 3PFX). The SELs A1 (V96–V101), A2 (T403–Q414), A3 (D373–Q377), A4 (T387–I396) and B1 (Y51–D57), B2 (P191–A196), B3 (G241–R248) and B4 (G342–D345) are colored in orange and yellow, respectively.

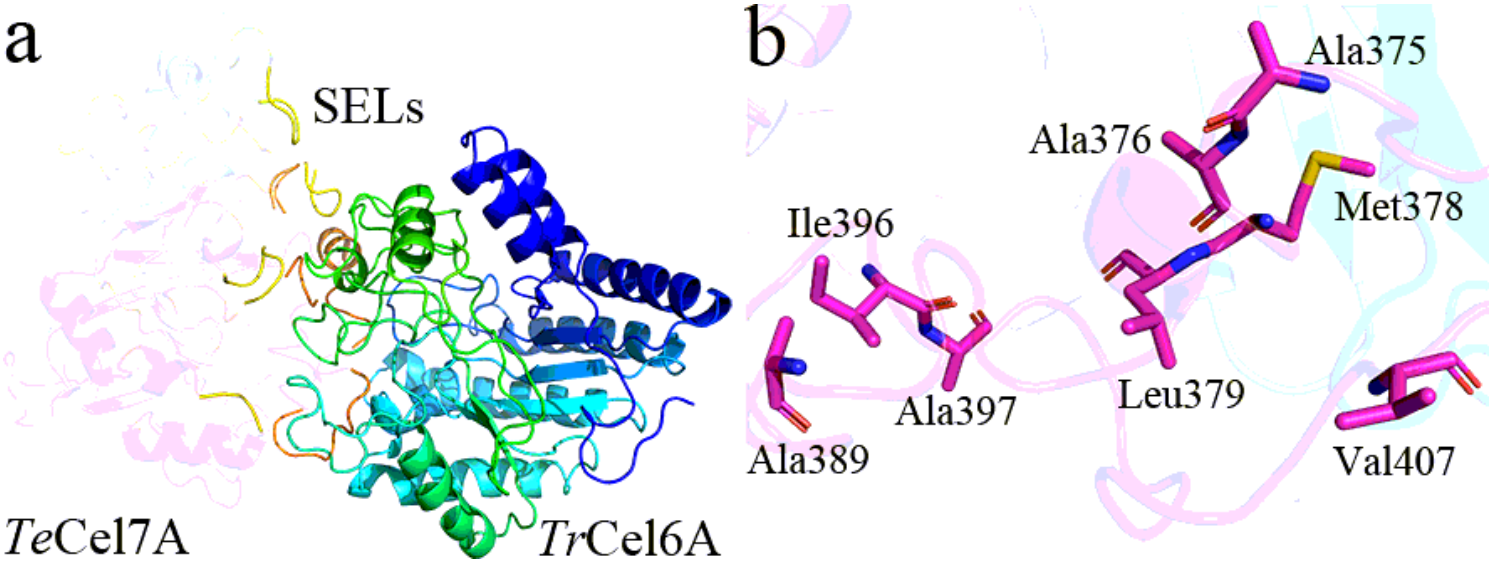

Figure 2

a) Optimal docking pose of TeCel7A–TrCel6A and b) hydrophobic residues of TeCel7A locate at the interactional interface, carbon, oxygen, nitrogen and sulfur of which are highlighted in pink, red, blue and yellow, respectively.

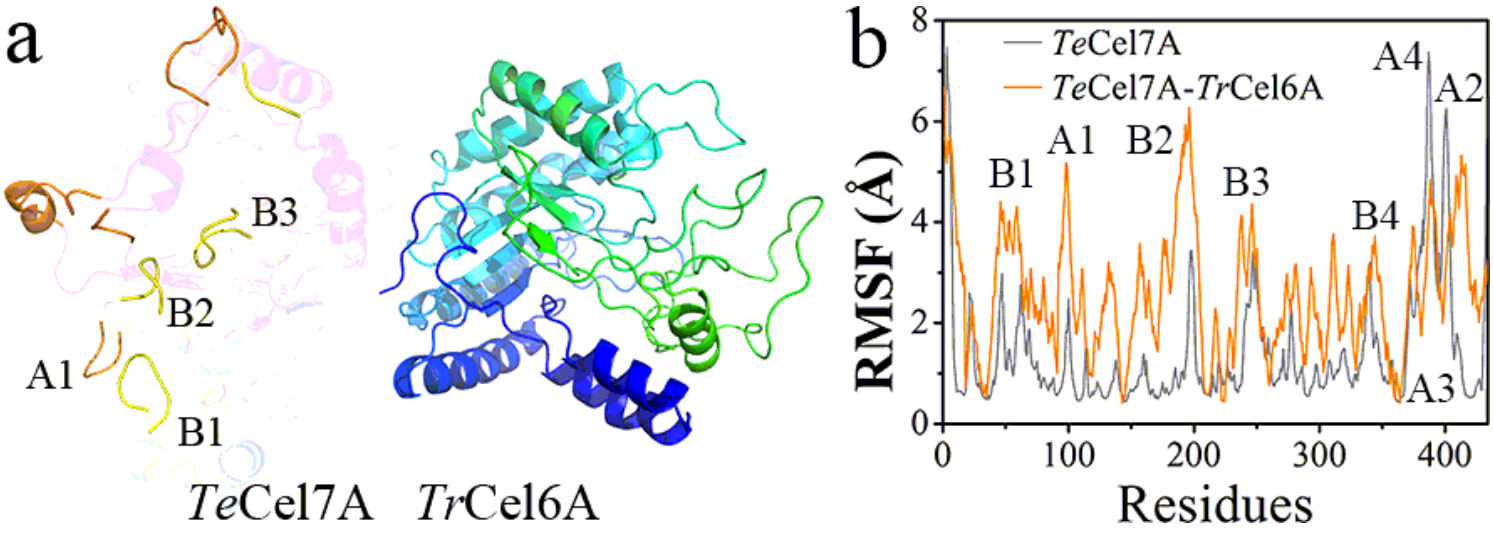

Figure 3

(a) Final pose of TeCel7A–TrCel6A after a 1.5-μs MD simulation; (b) RMSF of each residue in TeCel7A in free and bound states over the 1.5 μs MD trajectory for each.

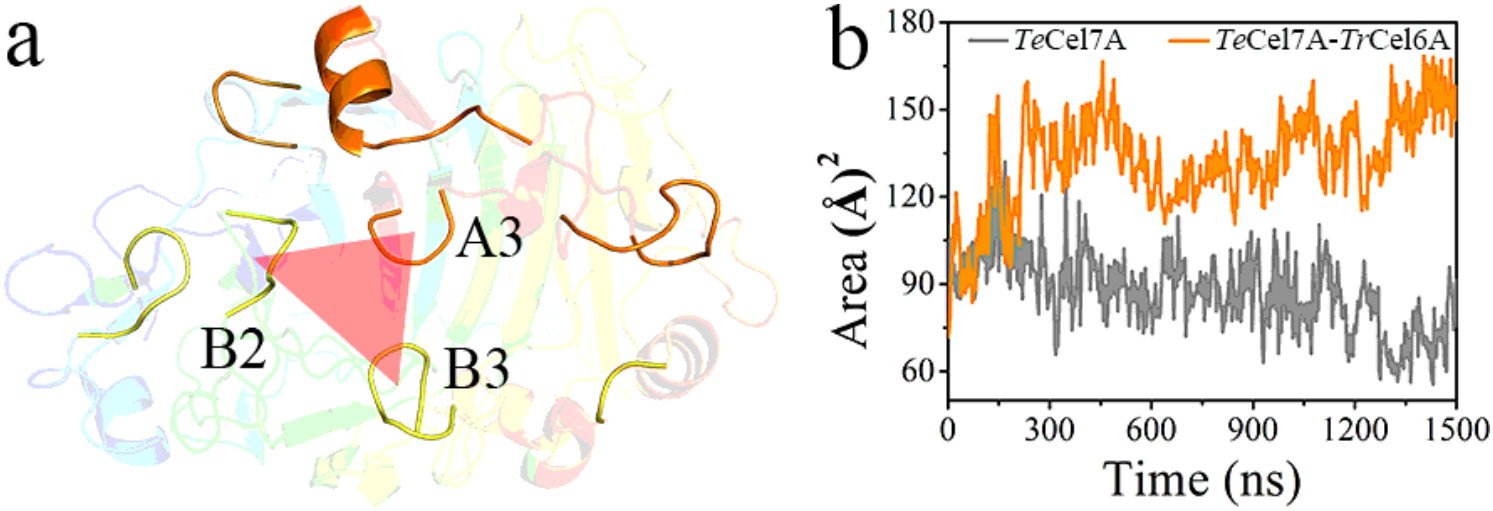

Figure 4

a) CSA highlighted by translucent red triangle is characterized by the size of the triangle connecting the COM of loops B2, B3 and A3. b) Time evolution of the CSA. The results are calculated over the 1.5 μs MD trajectories

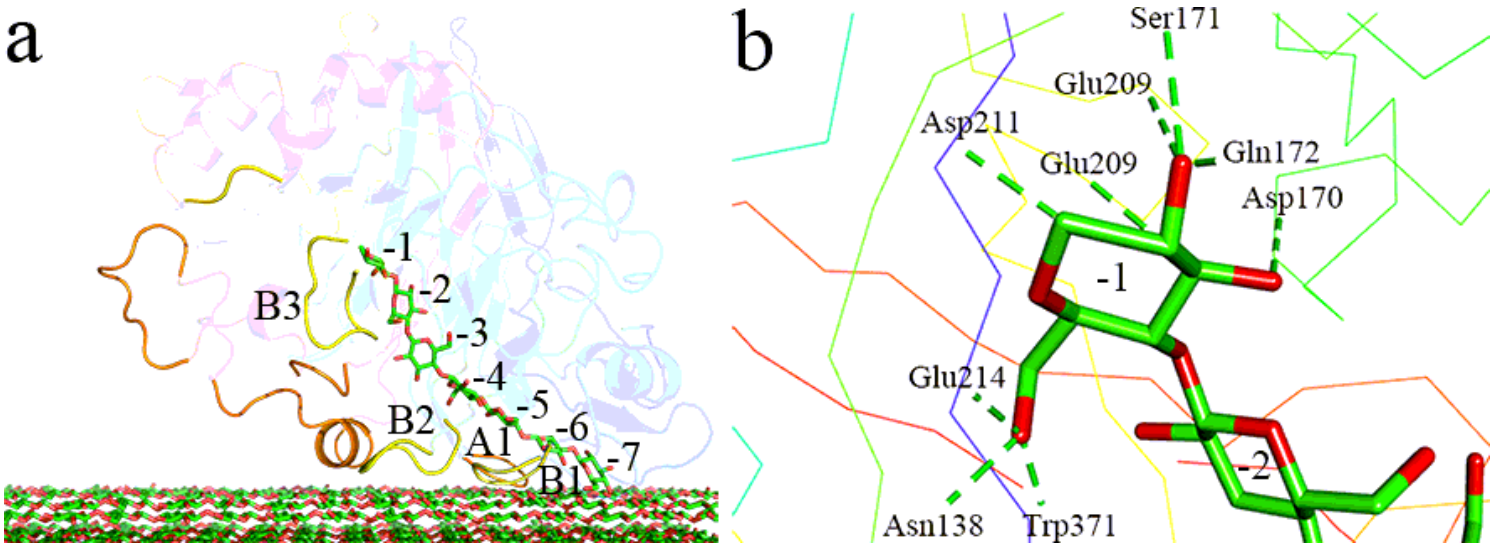

Figure 5

a) Schematic diagram of TeCel7A before dissociation from cellulose. b) Hydrogen bonds formed between −1 glucosyl ring and enzyme (simplified to line). Dethreading denotes that the enzyme slides off the cellulose chain (from −1 to −7) stage by stage. The hydrogen−bonding criteria are (i) the angle C−H···O > 135° and (ii) the distance C···O < 3.5 Å. C atoms of the polysaccharides are colored in green. Hydrogen bonds are shown in green dotted line.

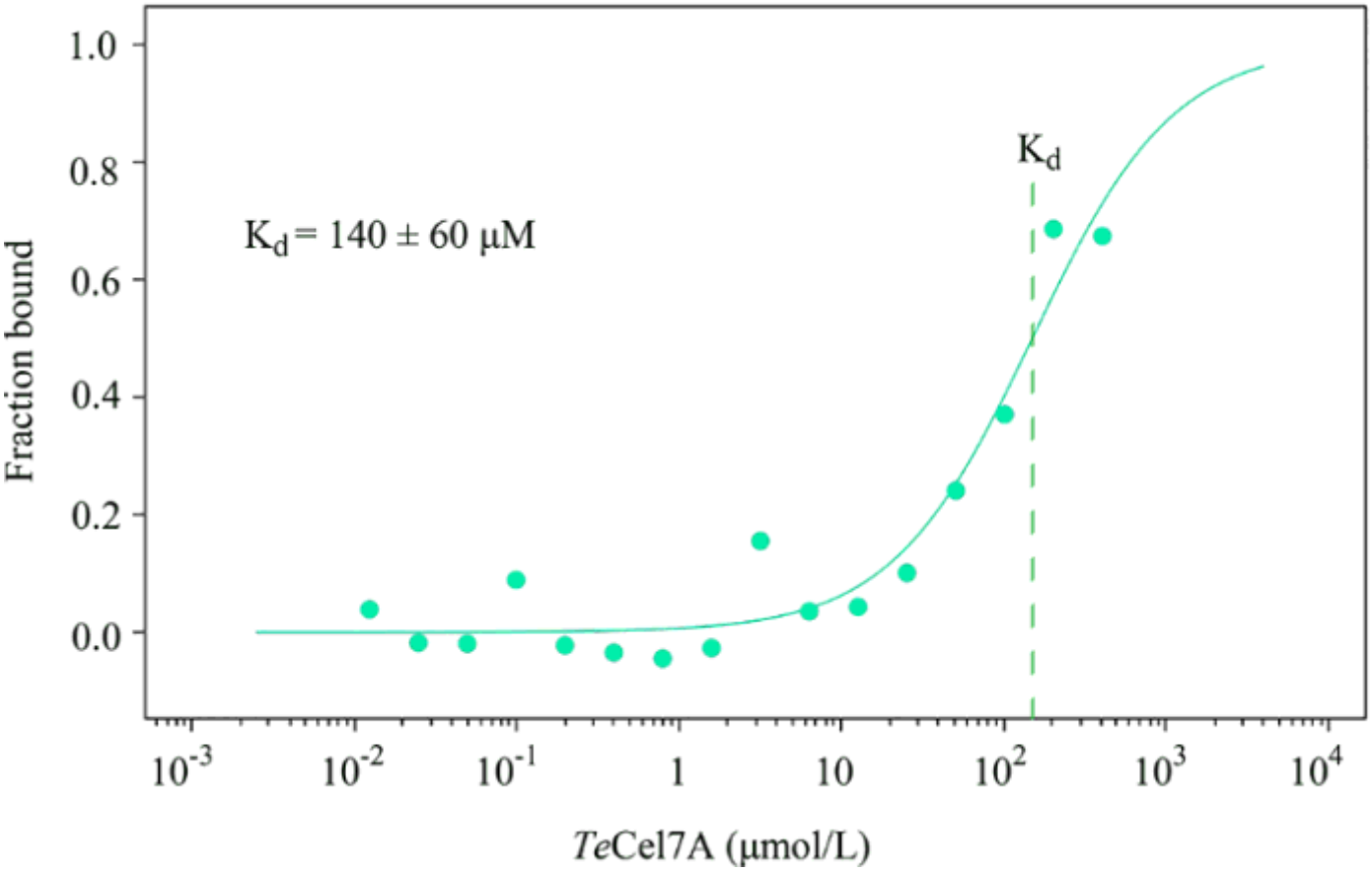

Figure 6

Fraction bound normalized MST binding curves and calculated Kd, characterizing the binding of TeCel7A to TrCel6A.

Supplementary Files

This is a list of supplementary files associated with this preprint. Click to download.

- GraphicalAbstract.png
- SupportingInformation.docx